Digital Signal Processing 78 (2018) 175–184

Contents lists available at ScienceDirect

Digital Signal Processing

www.elsevier.com/locate/dsp

Computationally efficient direction of arrival estimation with unknown number of signals

Feng-Gang Yan, Jun Wang, Shuai Liu *, Bin Cao *, Ming Jin

ARTICLE INFO

Article history:
Available online 22 March 2018

Keywords:
Direction of arrival (DOA) estimation
Real part Capon (R-Capon)
Real-valued computation
Virtual signal model

ABSTRACT

In this paper, we investigate the problem of direction of arrival (DOA) estimation with unknown number of signals in the framework of beamforming. We show that the real part of the array output covariance matrix (R-AOCM) can be reformulated as an entire AOCM of a virtual array with available signal model for fast DOA estimate. By introducing an optimization problem to minimize the variance of the weighted output of this virtual array, DOA can be found by a novel real-valued real part Capon (R-Capon) estimator accordingly. Moreover, we prove that the rank of the R-AOCM is always no less than that of the entire AOCM, which suggests that R-Capon outperforms the standard Capon in scenarios with small numbers of snapshots. We also prove that the inverse of the R-AOCM can be equivalently jointed by those of two sub-matrices of about half sizes, and hence R-Capon has a significantly reduced computational complexity. These advantages as well as the theoretical analysis are finally verified by numerical simulations over a wide range of scenarios.

1. Introduction

It is of great interest to find the direction-of-arrivals (DOAs) of multiple narrow-band signals in many applications such as radar, sonar, passive localization and wireless communication [1] [2]. Over the past several decades, a variety of super-resolution subspace-based algorithms including multiple signal classification (MUSIC) [3], estimation of signal parameters via rotational invariance techniques (ESPRIT) [4] and their numerous derivations have been proposed [5–10]. Among those techniques most are based on eigenstructure analysis, in which the determination of effective rank of the array output covariance matrix (AOCM) is generally required to distinguish the exact signal- and the noise- subspaces, which is hard to be established without a prior knowledge of the signal environment [11] [12]. If the number of sources is incorrectly estimated, the performance of those subspace-based algorithms will deteriorate significantly [13–16].

Akaike information criterion (AIC) and minimum description length (MDL) [20] are two of the most important methods for determining the number of sources. Unfortunately, numerical experimental evidence shows that they do indeed tend to estimate a wrong number of components for a small number of snapshots and a low signal-to-noise ratio (SNR), and hence their performance may be not satisfying in practice [21]. In order to estimate source DOAs without knowing the number of sources, many other approaches without source number detection have been proposed recently [22] [23]. Nevertheless, these techniques are inefficient and computationally intensive, which may be too expensive for real-time applications.

Beamforming techniques can be applied to solve the DOA estimation problem without knowing the number of signals [24] [25]. One of the most popular beamformers is the minimum variance distortionless response (MVDR) (also known as Capon) [26–28]. The primary advantage of the Capon algorithm is its easy application with no dependence on array configurations as well as close performance to MUSIC [31]. However, the conventional Capon involves a spectral search requiring to compute the product of the steering vector and the inverse of the entire AOCM. Because both the steering vector and the AOCM are generally modeled as complex-valued, this spectral search requires expensive complex-valued computations accordingly.

In this paper, we focus on the problem of DOA estimation with unknown number of sources, where efficient real-valued computations are taken into account to reduce the computational complexity. We propose a novel Capon-like DOA estimator named the real part Capon (R-Capon) because it exploits only the real part of the AOCM (R-AOCM) instead of the entire AOCM. The proposed method can be used for fast DOA estimation with significantly reduced complexity. Here, we briefly summarize the contributions of this paper.

1) Unlike most state-of-the-art algorithms which generally consider the problem of DOA estimation based on conventional

* Corresponding author.
E-mail addresses: liu_shuai_boy@163.com (S. Liu), caobin@hit.edu.cn (B. Cao).

https://doi.org/10.1016/j.dsp.2018.03.012
1051-2004/

signal models resulted from the entire AOCM, a new virtual signal model based on only the R-AOCM is established. It is shown that this virtual signal model can be further used to find signal DOAs because the R-AOCM can be reformulated as an entire AOCM of a virtual array equivalently.

2) A novel modification of the conventional Capon beamformer is proposed for DOA estimation without knowing the number of signals. Compared with the standard Capon, the proposed method exploits only the R-AOCM instead of the entire AOCM and it only requires to compute the inverse of the real matrix R-AOCM. Furthermore, two theorems are provided to show that the inverse of the R-AOCM can be equivalently jointed by those of two sub-matrices of about half sizes, and hence the proposed algorithm in fact has a significantly reduced computational burden as compared to Capon.
3) The rank of the R-AOCM is found to be always no less than that of the entire AOCM, and the proposed technique are found to outperform the standard Capon with small numbers of snapshots. As a result, the proposed estimator obtains reduced computational complexity with improved accuracy as compared to the conventional Capon in such scenarios.

The remainder of this paper is organized as follows. The signal model for DOA estimation with basic assumption as well as a brief review on the conventional Capon is given in section 2. In Section 3, the virtual signal model contained in the R-Capon is discussed, based on which the detailed derivations of the proposed R-Capon algorithm is described. Section 4 presents the theoretical analysis of the proposed method, in which three theorems providing insights into the rank of the R-AOCM and the inverse of the R-AOCM are proved. Numerical simulations are given in Section 5 to demonstrate the effectiveness of the proposed method and to verify the theoretical analysis, and the conclusions of this work are summarized in section 6.

Mathematical notations: Throughout the paper, matrices and vectors are denoted by upper- and lower- boldface letters, respectively. Complex- and real- vectors and matrices are denoted by single-bar- and double-bar- boldface letters, respectively. $\mathrm{Re}(\cdot)$ and $\mathrm{Im}(\cdot)$ stand for the real part- and the imaginary part- of the embraced element, respectively. In addition, $j=\sqrt{-1}$, $(\cdot)^*$ is conjugate, $(\cdot)^T$ is transpose, $(\cdot)^H$ is conjugate transpose, $E[\cdot]$ is mathematical expectation, $\|\cdot\|_{\mathrm{F}}^2$ is Frobenius norm, $\mathrm{rank}(\cdot)$ is rank of the embraced matrix, $\mathbb{I}$ is the identity matrix, $\mathbf{0}$ is a matrix or vector with all zero elements, $\mathrm{diag}\{\cdot\}$ is a diagonal matrix composed of the embraced elements and $\mathbb{J}$ is the exchange matrix with ones on its anti-diagonal and zeros elsewhere.

2. Signal model and conventional capon

Assume that K uncorrelated narrow-band signals $s_k(t)$, $k\in[1,K]$ with unknown DOAs $\boldsymbol{\theta}\triangleq[\theta_1,\theta_2,\ldots,\theta_K]$ impinge from far-field on a uniform linear array (ULA) composed of M antenna elements simultaneously. In most subspace-based high-resolution DOA estimators, M is generally assumed to be larger than K [13] [29]. In the proposed technique, it is assumed $M>2K$, which is reasonable for large arrays [30]. Although this is more strict as compared to the conventional Capon, it is to be shown this assumption allows a significant reduction on complexity.

Let the first sensor be the reference point, the array output at snapshot $t, t\in[1,T]$ is given by [1–14]

$$\mathbf{x}(t)=\mathbf{A}(\boldsymbol{\theta})\mathbf{s}(t)+\mathbf{n}(t), \tag{1}$$

where $\mathbf{A}(\boldsymbol{\theta})=[\mathbf{a}(\theta_1),\mathbf{a}(\theta_2),\ldots,\mathbf{a}(\theta_K)]$ is the $M\times K$ array manifold with each column

$$\mathbf{a}(\theta)=\left[1,e^{j(2\pi/\lambda)d\sin\theta},\cdots,e^{j(2\pi/\lambda)d(M-1)\sin\theta}\right]^T \tag{2}$$

denoting the $M\times 1$ steering vector, where λ is the wavelength of the narrow-band signals. $\mathbf{n}(t)$ is the $M\times 1$ additive white Gaussian noise (AWGN) satisfying

$$\begin{cases} E[\mathbf{n}(t)\mathbf{n}^T(t)]=\mathbf{0} & \text{(a)}\\ E[\mathbf{n}(t)\mathbf{n}^H(t)]=\sigma_n^2\mathbb{I}, & \text{(b)}\end{cases} \tag{3}$$

where σ_n^2 is the noise power, $\mathbb{I}$ is the identity matrix. $\mathbf{s}(t)$ is the $K\times 1$ signal vector, which satisfies

$$\begin{cases} E[\mathbf{s}(t)\mathbf{s}^T(t)]=\mathbf{0} & \text{(a)}\\ E[\mathbf{s}(t)\mathbf{s}^H(t)]=\mathbb{S}, & \text{(b)}\end{cases} \tag{4}$$

where $\mathbf{0}$ is the zero matrix and $\mathbb{S}$ is an $M\times M$ real diagonal, denoting the source covariance matrix. Assumption (4) is made to guarantee that the incident signals are circular, which is commonly used as a standard hypothesis for narrow-band signal DOA estimate [17–19]. The $M\times M$ AOCM is given by

$$\mathbf{R}=\mathrm{E}[\mathbf{x}(t)\mathbf{x}^H(t)]=\mathbf{A}(\boldsymbol{\theta})\mathbb{S}\mathbf{A}^H(\boldsymbol{\theta})+\sigma_n^2\mathbb{I}. \tag{5}$$

In practice, the theoretical AOCM in (5) is unavailable, and we can use T snapshots of the observed data to obtain the estimated AOCM (EAOCM) as

$$\widehat{\mathbf{R}}=\frac{1}{T}\sum_{t=1}^{T}\mathbf{x}(t)\mathbf{x}^H(t). \tag{6}$$

If K is known or has been estimated by methods [20–23] in advance, subspace-based approaches such as MUSIC [3], ESPRIT [4] and their derivations [5–10] generally compute the eigenvalue decomposition (EVD) of the EAOCM to extract the exact signal- or noise- subspaces to derive different cost functions for further DOA estimate. It has been shown in [13] [14] that the performances of those techniques will deteriorate significantly if K is incorrectly estimated.

To avoid signal number detecting, the conventional Capon [26–31] defines a weighted array output $\mathbf{y}(t)=\mathbf{w}^H\mathbf{x}(t)$ and finds DOAs by minimizing the power of $\mathbf{y}(t)$ as

$$\min_{\mathbf{w}}\mathrm{E}[\mathbf{y}(t)\mathbf{y}^H(t)]=\mathbf{w}^H\mathbf{R}\mathbf{w},\quad \text{s.t. } \mathbf{w}^H\mathbf{a}(\theta)=1. \tag{7}$$

By solving (7), DOAs can be found by searching the peaks of

$$f_{\mathrm{Capon}}(\theta)=\frac{1}{\mathbf{a}^H(\theta)\widehat{\mathbf{R}}^{-1}\mathbf{a}(\theta)} \tag{8}$$

over $[-\pi/2,\pi/2]$. The peak number of $f_{\mathrm{Capon}}(\theta)$ gives signal amount while the peak locations indicate signal DOAs.

3. Proposed R-Capon algorithm

3.1. Virtual signal model

We are to show in this subsection that the R-AOCM contains a virtual signal model available for DOA estimate. Let $\mathbb{R}_{\mathrm{re}}\triangleq\mathrm{Re}(\mathbf{R})$. Using $\mathbb{R}_{\mathrm{re}}=\frac{1}{2}(\mathbf{R}+\mathbf{R}^*)$ and (5), we have

$$\begin{aligned}\mathbb{R}_{\mathrm{re}}&=\frac{1}{2}[\mathbf{A}(\boldsymbol{\theta})\mathbb{S}\mathbf{A}^H(\boldsymbol{\theta})+\mathbf{A}^*(\boldsymbol{\theta})\mathbb{S}\mathbf{A}^T(\boldsymbol{\theta})]+\sigma_n^2\mathbb{I}\\&=\underbrace{[\mathbf{A}(\boldsymbol{\theta})\ \mathbf{A}^*(\boldsymbol{\theta})]}_{M\times 2K}\times\underbrace{\frac{1}{2}\begin{bmatrix}\mathbb{S}&\mathbf{0}\\ \mathbf{0}&\mathbb{S}\end{bmatrix}}_{2K\times 2K}\times\underbrace{\begin{bmatrix}\mathbf{A}^H(\boldsymbol{\theta})\\ \mathbf{A}^T(\boldsymbol{\theta})\end{bmatrix}}_{2K\times M}+\sigma_n^2\mathbb{I}\\&=\widetilde{\mathbf{A}}(\boldsymbol{\theta})\widetilde{\mathbb{S}}\widetilde{\mathbf{A}}^H(\boldsymbol{\theta})+\sigma_n^2\mathbb{I},\end{aligned} \tag{9}$$

where matrices $\widetilde{\mathbb{S}} \in \mathbb{R}^{2K\times 2K}$ and $\widetilde{\mathbf{A}}(\boldsymbol{\theta}) \in \mathbb{C}^{M\times 2K}$ are defined as

$$\widetilde{\mathbb{S}} = \frac{1}{2}\begin{bmatrix} \mathbb{S} & \mathbf{0} \\ \mathbf{0} & \mathbb{S} \end{bmatrix} \tag{10-1}$$

$$\widetilde{\mathbf{A}}(\boldsymbol{\theta}) = \left[\mathbf{A}(\boldsymbol{\theta})\ \mathbf{A}^*(\boldsymbol{\theta})\right]. \tag{10-2}$$

Using (4), we can rewrite $\widetilde{\mathbb{S}}$ as

$$\begin{aligned}\widetilde{\mathbb{S}} &= \mathrm{E}\left\{ \underbrace{\begin{bmatrix} \mathbf{s}(t) \\ \mathbf{s}^*(t) \end{bmatrix}}_{2K\times 1} \times \underbrace{\left[\mathbf{s}^H(t)\ \mathbf{s}^T(t)\right]}_{1\times 2K} \right\} \\ &= \mathrm{E}[\widetilde{\mathbf{s}}(t)\widetilde{\mathbf{s}}^H(t)],\end{aligned} \tag{11}$$

where

$$\widetilde{\mathbf{s}}(t) = \begin{bmatrix} \mathbf{s}(t) \\ \mathbf{s}^*(t) \end{bmatrix} \in \mathbb{C}^{2K\times 1}. \tag{12}$$

Inserting (11) into (9) and using (3) leads to

$$\begin{aligned}\mathbb{R}_{\mathrm{re}} &= \widetilde{\mathbf{A}}(\boldsymbol{\theta})\widetilde{\mathbb{S}}\widetilde{\mathbf{A}}^H(\boldsymbol{\theta}) + \sigma_n^2\mathbb{I} \\ &= \widetilde{\mathbf{A}}(\boldsymbol{\theta})\,\mathrm{E}[\widetilde{\mathbf{s}}(t)\widetilde{\mathbf{s}}^H(t)]\widetilde{\mathbf{A}}(\boldsymbol{\theta})^H + \mathrm{E}\left[\mathbf{n}(t)\mathbf{n}^H(t)\right] \\ &= \mathrm{E}\left\{\left[\widetilde{\mathbf{A}}(\boldsymbol{\theta})\widetilde{\mathbf{s}}(t) + \mathbf{n}(t)\right]\left[\widetilde{\mathbf{A}}(\boldsymbol{\theta})\widetilde{\mathbf{s}}(t) + \mathbf{n}(t)\right]^H\right\} \\ &= \mathrm{E}\left[\widetilde{\mathbf{x}}(t)\widetilde{\mathbf{x}}^H(t)\right],\end{aligned} \tag{13}$$

where $\widetilde{\mathbf{x}}(t)$ is a $M \times 1$ vector, given by

$$\widetilde{\mathbf{x}}(t) = \widetilde{\mathbf{A}}(\boldsymbol{\theta})\widetilde{\mathbf{s}}(t) + \mathbf{n}(t). \tag{14}$$

Comparing (14) with (1) as well as comparing (13) with (5), one concludes that the R-AOCM can be equivalently regarded as an entire AOCM of the received data by a virtual array with a virtual manifold $\widetilde{\mathbf{A}}(\boldsymbol{\theta})$. The observed data by this virtual array is $\widetilde{\mathbf{x}}(t)$, the incident signal on this virtual array is $\widetilde{\mathbf{s}}(t)$ and the signal covariance matrix is $\widetilde{\mathbb{S}}$.

Remark 1. Similarly, we can obtain another virtual signal model for the imaginary part of the AOCM. By defining

$$\mathbb{R}_{\mathrm{im}} \triangleq \mathrm{Im}(\mathbf{R}) \in \mathbb{R}^{M\times M} \tag{15-1}$$

$$\mathbb{S}_2 \triangleq \frac{j}{2}\begin{bmatrix} \mathbb{S} & \mathbf{0} \\ \mathbf{0} & -\mathbb{S} \end{bmatrix} \in \mathbb{C}^{2K\times 2K} \tag{15-2}$$

$$\mathbf{A}_2(\boldsymbol{\theta}) \triangleq \left[\mathbf{A}^*(\boldsymbol{\theta}) \quad \mathbf{A}(\boldsymbol{\theta})\right] \in \mathbb{C}^{M\times 2K} \tag{15-3}$$

$$\mathbf{s}_2(t) \triangleq \frac{1}{2}\begin{bmatrix} (1+j)\mathbf{s}(t) \\ (1-j)\mathbf{s}^*(t) \end{bmatrix} \in \mathbb{C}^{2K\times 1}, \tag{15-4}$$

it can be easily verified that

$$\begin{cases} \mathbf{x}_2(t) = \mathbf{A}_2(\boldsymbol{\theta})\mathbf{s}_2(t) + \mathbf{n}(t) & \text{(a)} \\ \mathbb{R}_{\mathrm{im}} + \sigma_n^2\mathbb{I} = \mathrm{E}\left[\mathbf{x}_2(t)\mathbf{x}_2^H(t)\right]. & \text{(b)} \end{cases} \tag{16}$$

Hence, $\mathbb{R}_{\mathrm{im}} + \sigma_n^2\mathbb{I}$ can be also regarded as an entire AOCM of the data received by a virtual array with manifold $\mathbf{A}_2(\boldsymbol{\theta})$. The virtual observed data is $\mathbf{x}_2(t)$ while the incident signal is $\mathbf{s}_2(t)$ with its covariance matrix given by $\mathbb{S}_2$. □

3.2. Proposed algorithm

Following the idea of beamforming and using the virtual signal model in (14), we can similarly define a weighted output $\mathbf{y}_1(t) = \mathbf{w}^H\mathbf{x}_1(t)$ of the virtual array, and obtain the following optimization problem for DOA estimation

$$\min_{\mathbf{w}} \mathrm{E}\left[\mathbf{y}_1(t)\mathbf{y}_1^H(t)\right] = \mathbf{w}^H\mathbb{R}_{\mathrm{re}}\mathbf{w} \tag{17-1}$$

$$\text{s.t. } \mathbf{w}^H\widetilde{\mathbf{a}}(\theta) = 1, \tag{17-2}$$

where $\widetilde{\mathbf{a}}(\theta)$ is a virtual steering vector associated with the virtual manifold $\widetilde{\mathbf{A}}(\boldsymbol{\theta})$. Notice that $\forall\boldsymbol{\theta}$, $\mathbf{A}^*(\boldsymbol{\theta}) = \mathbf{A}(-\boldsymbol{\theta})$, therefore $\widetilde{\mathbf{A}}(\boldsymbol{\theta}) = \left[\mathbf{A}(\boldsymbol{\theta})\ \mathbf{A}(-\boldsymbol{\theta})\right]$ can be equivalently regarded as a combined manifold covering $\mathbf{A}(\boldsymbol{\theta})$ and $\mathbf{A}(-\boldsymbol{\theta})$. Consequently, $\widetilde{\mathbf{a}}(\theta)$ can be equivalently regarded as a combined steering vector covering $\mathbf{a}(\theta)$ and $\mathbf{a}(-\theta)$. Since $\mathbf{a}(\theta)$ and $\mathbf{a}(-\theta)$ are symmetrical, (17) can be simplified as[1]

$$\min_{\mathbf{w}} \mathbf{w}^H\mathbb{R}_{\mathrm{re}}\mathbf{w} \tag{18-1}$$

$$\text{s.t. } \mathbf{w}^H\mathbf{a}(\theta) = 1. \tag{18-2}$$

Now, we use the Lagrange multiplier technique and obtain

$$f(\mathbf{w}) = \mathbf{w}^H\mathbb{R}_{\mathrm{re}}\mathbf{w} - \mu\left[\mathbf{w}^H\mathbf{a}(\theta) - 1\right], \tag{19}$$

where μ is the Lagrange multiplier. By letting $\partial f(\mathbf{w})/\partial\mathbf{w} = 0$, it can be shown the optimal solution for (19) is given by

$$\mathbf{w}_{\mathrm{opt}} = \frac{\mathbb{R}_{\mathrm{re}}^{-1}\mathbf{a}(\theta)}{\mathbf{a}^H(\theta)\mathbb{R}_{\mathrm{re}}^{-1}\mathbf{a}(\theta)}. \tag{20}$$

Inserting (20) into the objective function $\mathbf{w}^H\mathbb{R}_{\mathrm{re}}\mathbf{w}$, the proposed R-Capon cost function is finally given by

$$f_{\mathrm{R-Capon}}(\theta) = \frac{1}{\mathbf{a}^H(\theta)\widehat{\mathbb{R}}_{\mathrm{re}}^{-1}\mathbf{a}(\theta)}. \tag{21}$$

Remark 2. Suppose that $\widehat{\theta}$ is a minimum of $f_{\mathrm{R-Capon}}(\theta)$ over $[0, \pi/2]$. Because $\widehat{\mathbb{R}}_{\mathrm{re}}^{-1}$ is a real matrix, we see from (21) that either $\widehat{\theta}$ or $-\widehat{\theta}$ is a true DOA since $f_{\mathrm{R-Capon}}(-\widehat{\theta}) = f_{\mathrm{R-Capon}}(-\widehat{\theta})$ (note that $\widehat{\theta}$ and $-\widehat{\theta}$ may be two true DOAs simultaneously if two distinct signals incident at $\widehat{\theta}$ and $-\widehat{\theta}$ coincidentally). Therefore, we can search $f_{\mathrm{R-Capon}}(\theta)$ over only $[0, \pi/2]$ (or $[-\pi/2, 0]$) with compressed search range to get the candidate angle $\widehat{\theta}$ (or $-\widehat{\theta}$), and then select between $\widehat{\theta}$ and $-\widehat{\theta}$ for correct DOA estimation. To solve the ambiguity problem with low complexity, the conventional beamformer (CBF) [1] [24] [25] can be applied to select the true DOA between $\widehat{\theta}$ and $-\widehat{\theta}$ by maximizing $\|\mathbf{a}^H(\theta)\widehat{\mathbf{R}}\mathbf{a}(\theta)\|$ [32]. □

Remark 3. Based on (16), we can define another weighted output $\mathbf{y}_2(t) = \mathbf{w}^H\mathbf{x}_2(t)$ and minimize the power of $\mathbf{y}_2(t)$ by

$$\min_{\mathbf{w}} \mathrm{E}\left[\mathbf{y}_2(t)\mathbf{y}_2^H(t)\right] = \mathbf{w}^H\mathbb{R}_{\mathrm{im}}\mathbf{w} + \sigma_n^2\|\mathbf{w}\|^2 \tag{22-1}$$

$$\text{s.t. } \mathbf{w}^H\mathbf{a}_2(\theta) = 1, \tag{22-2}$$

where again, $\mathbf{a}_2(\theta)$ is defined as a virtual steering vector covering both $\mathbf{a}(\theta)$ and $\mathbf{a}(-\theta)$, and (22) is simplified as

$$\min_{\mathbf{w}} \mathbf{w}^H\mathbb{R}_{\mathrm{im}}\mathbf{w} + \sigma_n^2\|\mathbf{w}\|^2 \tag{23-1}$$

$$\text{s.t. } \mathbf{w}^H\mathbf{a}(\theta) = 1. \tag{23-2}$$

By similarly using the Lagrange multiplier technique to solve (23), we obtain the following cost function

$$h(\theta) = \frac{1}{\mathbf{a}^H(\theta)\left[\widehat{\mathbb{R}}_{\mathrm{im}} + \widehat{\sigma}_n^2\mathbb{I}\right]^{-1}\mathbf{a}(\theta)}. \tag{24}$$

[1] The simplification leads to an estimation ambiguity problem, which is analyzed and solved in Remark 2 of this subsection.

By searching the minima of $h(\theta)$ over only half of the total angular field-of-view $[0, \pi/2]$ (or $[-\pi/2, 0]$), DOAs can be estimated by similarly exploiting the above ambiguity solving scheme. However, as (24) contains an additional noise part $\widehat{\sigma}_n^2\mathbb{I}$ which should be estimated in advance, we suggest to use the proposed R-Capon algorithm rather (24) in practice. □

4. Rank enhancement and complexly reduction

4.1. Rank enhancement

Comparing (21) with (8), one may predict that the proposed algorithm performs worse than the conventional Capon since half of the EAOCM information is lost in R-Capon. However, it is to be shown in the simulation part that the proposed method in fact has a similar performance to Capon. In addition, the following theorem suggests that in scenarios with small numbers of snapshots, the proposed technique outperforms the conventional Capon beyond expectation.

Proposition 1. *Let $\widehat{\mathbf{R}}$ be computed by (6) and let $\widehat{\mathbb{R}}_{\rm re} \triangleq {\rm Re}(\widehat{\mathbf{R}})$, we have*

$$\mathrm{rank}\big(\widehat{\mathbb{R}}_{\rm re}\big) \geqslant \mathrm{rank}\big(\widehat{\mathbf{R}}\big). \tag{25}$$

Proof. Since $\widehat{\mathbf{R}} = \frac{1}{T}\sum_{t=1}^{T}\mathbf{x}(t)\mathbf{x}^H(t)$, we can write $\widehat{\mathbf{R}} = \frac{1}{T}\mathbf{X}\mathbf{X}^H$, where $\mathbf{X} \triangleq [\mathbf{x}(1)\ \mathbf{x}(2)\ \cdots\ \mathbf{x}(T)]$ is an $M \times T$ direct-data matrix. According to matrix theory [26], we have

$$\mathrm{rank}\big(\widehat{\mathbf{R}}\big) = \mathrm{rank}\big(\mathbf{X}\big). \tag{26}$$

Using $\widehat{\mathbb{R}}_{\rm re} = \frac{1}{2}\big(\widehat{\mathbf{R}} + \widehat{\mathbf{R}}^*\big)$, we can write

$$\widehat{\mathbb{R}}_{\rm re} = \frac{1}{2T}\underbrace{\big[\mathbf{X}\ \mathbf{X}^*\big]}_{M\times 2T} \times \underbrace{\begin{bmatrix}\mathbf{X}^H\\ \mathbf{X}^T\end{bmatrix}}_{2T\times M} = \frac{1}{2T}\widetilde{\mathbf{X}}_1\widetilde{\mathbf{X}}_1^H, \tag{27}$$

and obtain $\mathrm{rank}\big(\widehat{\mathbb{R}}_{\rm re}\big) = \mathrm{rank}\big(\widetilde{\mathbf{X}}_1\big)$, where $\widetilde{\mathbf{X}}_1 = [\mathbf{X}\ \mathbf{X}^*]$ is as an $M \times 2T$ virtual direct-data matrix. Because $\widetilde{\mathbf{X}}_1$ is an augmented matrix as compared to $\mathbf{X}$, we have $\mathrm{rank}\big(\widetilde{\mathbf{X}}_1\big) \geqslant \mathrm{rank}\big(\mathbf{X}\big)$, and $\mathrm{rank}\big(\widehat{\mathbb{R}}_{\rm re}\big) \geqslant \mathrm{rank}\big(\widehat{\mathbf{R}}\big)$ holds accordingly. □

It is observed from (26) that $\mathrm{rank}\big(\widehat{\mathbf{R}}\big)$ depends on the linear independence of the columns of $\mathbf{X}$. When T is sufficiently large such that there are at least M linear independent columns in $\mathbf{X}$, there must also be at least M linear independent columns in $\widetilde{\mathbf{X}}_1$ since the latter matrix is augmented. In such cases, both $\widehat{\mathbf{R}}$ and $\widehat{\mathbb{R}}_{\rm re}$ are of full ranks, and we have $\mathrm{rank}\big(\widehat{\mathbb{R}}_{\rm re}\big) = \mathrm{rank}\big(\widehat{\mathbf{R}}\big) = M$. Oppositely, when T is too mall such that there are less than M linear independent columns in $\mathbf{X}$, $\widehat{\mathbf{R}}$ is of rank defect. In such cases, the conventional Capon spectral may show pseudo peaks, and its performance may deteriorate significantly. According to Theorem 1, the proposed R-Capon may outperform the conventional Capon since $\widehat{\mathbb{R}}_{\rm re}$ is rank-enhanced. In fact, it is to be shown in the simulation result section that the proposed method does outperform the conventional Capon with small T's.

Remark 4. Let $\widehat{\mathbb{R}}_{\rm im} \triangleq {\rm Re}\big(\widehat{\mathbf{R}}\big)$. Using $\widehat{\mathbb{R}}_{\rm im} = \frac{j}{2}\big(\widehat{\mathbf{R}}^* - \widehat{\mathbf{R}}\big)$ and $\widehat{\mathbf{R}} = \frac{1}{T}\mathbf{X}\mathbf{X}^H$, we can write

$$\widehat{\mathbb{R}}_{\rm im} = \frac{j}{2T}\underbrace{\big[\mathbf{X}^*\ j\mathbf{X}\big]}_{M\times 2T}\underbrace{\begin{bmatrix}\mathbf{X}^T\\ j\mathbf{X}^H\end{bmatrix}}_{2T\times M} = \frac{1}{2T}\widetilde{\mathbf{X}}_2\widetilde{\mathbf{X}}_2^H, \tag{28}$$

and obtain $\mathrm{rank}\big(\widehat{\mathbb{R}}_{\rm im}\big) = \mathrm{rank}\big(\widetilde{\mathbf{X}}_2\big)$. Because $\mathrm{rank}\big(\widetilde{\mathbf{X}}_2\big) \geqslant \mathrm{rank}\big(\mathbf{X}\big) = \mathrm{rank}\big(\widehat{\mathbf{R}}\big)$, we obtain from (28) that

$$\mathrm{rank}\big(\widehat{\mathbb{R}}_{\rm im}\big) \geqslant \mathrm{rank}\big(\widehat{\mathbf{R}}\big). \tag{29}$$

In addition, by decomposing $\widehat{\sigma}_n^2\mathbb{I}$ as $\widehat{\sigma}_n^2\mathbb{I} = \mathbb{B}\mathbb{B}^T$, where $\mathbb{B} = \mathrm{diag}\{\widehat{\sigma}_n, \widehat{\sigma}_n, \cdots, \widehat{\sigma}_n\}$, we can write

$$\widehat{\mathbb{R}}_{\rm im} + \widehat{\sigma}_n^2\mathbb{I} = \frac{j}{2T}\underbrace{\big[\widetilde{\mathbf{X}}_2\ \gamma\mathbb{B}\big]}_{M\times(2T+M)}\underbrace{\begin{bmatrix}\widetilde{\mathbf{X}}_2^T\\ \gamma\mathbb{B}^T\end{bmatrix}}_{(2T+M)\times M} = \frac{j}{2T}\widetilde{\mathbf{X}}_3\widetilde{\mathbf{X}}_3^H, \tag{30}$$

where $\widetilde{\mathbf{X}}_3 = \big[\widetilde{\mathbf{X}}_2\ \gamma\mathbb{B}\big]$ is another $M \times (2T + M)$ augmented matrix, and $\gamma = \sqrt{\frac{2T}{j}} = \frac{2\sqrt{T}}{(1+j)}$ is a scale coefficient. Since $\mathrm{rank}\big(\widetilde{\mathbf{X}}_3\big) \geqslant \mathrm{rank}\big(\widetilde{\mathbf{X}}_2\big) \geqslant \mathrm{rank}\big(\widehat{\mathbf{R}}\big)$, it follows from (30) that

$$\mathrm{rank}\big(\widehat{\mathbb{R}}_{\rm im} + \widehat{\sigma}_n^2\mathbb{I}\big) \geqslant \mathrm{rank}\big(\widehat{\mathbf{R}}\big). \tag{31}$$

Therefore, the cost function $h(\theta)$ in (24) may also outperforms the conventional capon with small T's. □

4.2. Complexity reduction

As $\mathbb{S}$ is diagonal, one can prove that $\mathbf{R}$ is centro-Hermitian such that $\mathbb{J}\mathbf{R}\mathbb{J} = \mathbf{R}^*$ and $\mathbb{J}\mathbf{R}^*\mathbb{J} = \mathbf{R}$ [34–38]. Using these facts, we have

$$\begin{cases}\mathbb{R}_{\rm re}^T = \mathbb{R}_{\rm re} & (a)\\ \mathbb{J}\mathbb{R}_{\rm re}\mathbb{J} = \mathbb{R}_{\rm re}. & (b)\end{cases} \tag{32}$$

Therefore, $\mathbb{R}_{\rm re}$ is a bisymmetric matrix, and it is symmetrical about both of its main diagonals [33]. Based on such a mathematical fact, we have the following two theorems which suggest that $\mathbb{R}_{\rm re}^{-1}$ can be efficiently jointed by the inverses of two sub-matrices of about half sizes, and therefore the computational complexity is significantly reduced.

Theorem 1. *When M is an even number such that $M = 2k$, $\mathbb{R}_{\rm re}$ can be divided into four $k \times k$ sub-matrices as*

$$\mathbb{R}_{\rm re} = \begin{bmatrix}(\mathbb{R}_{\rm re})_{11} & (\mathbb{R}_{\rm re})_{21}^T\\ (\mathbb{R}_{\rm re})_{21} & \mathbb{J}\,(\mathbb{R}_{\rm re})_{11}\,\mathbb{J}\end{bmatrix}. \tag{33}$$

In addition, the inverse of $\mathbb{R}_{\rm re}$ is given by

$$\mathbb{R}_{\rm re}^{-1} = \frac{1}{2}\begin{bmatrix}\mathbb{H}_1^{-1} + \mathbb{H}_2^{-1} & \left(\mathbb{H}_2^{-1} - \mathbb{H}_1^{-1}\right)\mathbb{J}\\ \mathbb{J}\left(\mathbb{H}_2^{-1} - \mathbb{H}_1^{-1}\right) & \mathbb{J}\left(\mathbb{H}_1^{-1} + \mathbb{H}_2^{-1}\right)\mathbb{J}\end{bmatrix}, \tag{34}$$

where $\mathbb{H}_1$ and $\mathbb{H}_2$ are two $k \times k$ sub-matrices, given by

$$\mathbb{H}_1 \triangleq (\mathbb{R}_{\rm re})_{11} - \mathbb{J}\,(\mathbb{R}_{\rm re})_{21} \tag{35-1}$$

$$\mathbb{H}_2 \triangleq (\mathbb{R}_{\rm re})_{11} + \mathbb{J}\,(\mathbb{R}_{\rm re})_{21}\,. \tag{35-2}$$

Proof. See Appendix A. □

Theorem 2. *When M is an odd number such that $M = 2k + 1$, $\mathbb{R}_{\rm re}$ can be divided as*

$$\mathbb{R}_{\rm re} = \begin{bmatrix}(\mathbb{R}_{\rm re})_{11} & \mathbb{b} & \mathbb{J}\,(\mathbb{R}_{\rm re})_{21}\,\mathbb{J}\\ \mathbb{b}^T & a & \mathbb{b}^T\mathbb{J}\\ (\mathbb{R}_{\rm re})_{21} & \mathbb{J}\mathbb{b} & \mathbb{J}\,(\mathbb{R}_{\rm re})_{11}\,\mathbb{J}\end{bmatrix}, \tag{36}$$

where a is scalar, $\mathbb{b}$ is a $k \times 1$ vector, $(\mathbb{R}_{\rm re})_{11}$ and $(\mathbb{R}_{\rm re})_{21}$ are two $k \times k$ sub-matrices. In addition, the inverse of $\mathbb{R}_{\rm re}$ is given by

$$\mathbb{R}_{\rm re}^{-1} = \frac{1}{2}\begin{bmatrix}\mathbb{H}_1^{-1} + \mathbb{K}_1\mathbb{H}_3^{-1}\mathbb{K}_1^T & \mathbb{H}_1^{-1}\mathbb{K}_2^T + \mathbb{K}_1\mathbb{H}_3^{-1}\mathbb{L}\\ \mathbb{K}_2\mathbb{H}_1^{-1} + \mathbb{L}\mathbb{H}_3^{-1}\mathbb{K}_1^T & \mathbb{K}_2\mathbb{H}_1^{-1}\mathbb{K}_2^T + \mathbb{L}\mathbb{H}_3^{-1}\mathbb{L}^T\end{bmatrix}, \tag{37}$$

where

Table 1
Complexity in terms of real-valued operations.

Algorithm \ Step	Inverse computation	Spectral search
Capon	$4\times\mathcal{O}(M^3)$	$4J\times\mathcal{O}(M^2+M))$
R-Capon	$1/4\times\mathcal{O}(M^3)$	$J/2\times\mathcal{O}(M^2+M))$

$$\mathbb{H}_3=\begin{bmatrix} a & \sqrt{2}\mathbb{b}^T \\ \sqrt{2}\mathbb{b} & \mathbb{H}_2 \end{bmatrix}\in\mathbb{R}^{(k+1)\times(k+1)} \tag{38}$$

$$\mathbb{K}_1=\begin{bmatrix}\mathbf{0} & \mathbb{I}\end{bmatrix}\in\mathbb{R}^{k\times(k+1)} \tag{39}$$

$$\mathbb{K}_2=\begin{bmatrix}\mathbf{0} & -\mathbb{J}\end{bmatrix}^T\in\mathbb{R}^{(k+1)\times k} \tag{40}$$

$$\mathbb{L}=\begin{bmatrix}\sqrt{2} & \mathbf{0}\\ \mathbf{0} & \mathbb{J}\end{bmatrix}\in\mathbb{R}^{(k+1)\times(k+1)}. \tag{41}$$

Proof. See Appendix B. □

Remark 5. Theorem 1 and Theorem 2 indicate that the theoretical $\mathbb{R}_{\text{re}}^{-1}$ can be jointed by two sub-matrices $\mathbb{H}_1^{-1}$ and $\mathbb{H}_2^{-1}$ with $M=2k$ or by $\mathbb{H}_1^{-1}$ and $\mathbb{H}_3^{-1}$ with $M=2k+1$. In practice, because of the finite numbers of snapshot $T<\infty$, the centro-Hermitian character does not hold for $\widehat{\mathbf{R}}$, and we generally have $\mathbb{J}\widehat{\mathbf{R}}\mathbb{J}\neq\widehat{\mathbf{R}}^*$ and $\mathbb{J}\widehat{\mathbf{R}}^*\mathbb{J}\neq\widehat{\mathbf{R}}$. Consequently, $\widehat{\mathbb{R}}_{\text{re}}$ is no longer bisymmetric such that

$$\mathbb{J}\widehat{\mathbb{R}}_{\text{re}}\mathbb{J}\neq\widehat{\mathbb{R}}_{\text{re}}. \tag{42}$$

Therefore, the above two theorems are not reasonable for $\widehat{\mathbb{R}}_{\text{re}}^{-1}$. To solve this problem, we consider the forward/backward (FB) averaging EAOCM (FB-EAOCM) [34] [35]

$$\widehat{\mathbf{R}}_{\text{FB}}=\frac{1}{2}\left(\widehat{\mathbf{R}}+\mathbb{J}\widehat{\mathbf{R}}^*\mathbb{J}\right). \tag{43}$$

Using $\mathbb{J}^2=\mathbb{I}$, we obtain from (43) that

$$\begin{cases}\mathbb{J}\widehat{\mathbf{R}}_{\text{FB}}\mathbb{J}=\frac{1}{2}\left(\mathbb{J}\widehat{\mathbf{R}}\mathbb{J}+\widehat{\mathbf{R}}^*\right)=\widehat{\mathbf{R}}_{\text{FB}}^* & \text{(a)}\\ \mathbb{J}\widehat{\mathbf{R}}_{\text{FB}}^*\mathbb{J}=\frac{1}{2}\left(\mathbb{J}\widehat{\mathbf{R}}^*\mathbb{J}+\widehat{\mathbf{R}}\right)=\widehat{\mathbf{R}}_{\text{FB}}. & \text{(b)}\end{cases} \tag{44}$$

Hence, $\widehat{\mathbf{R}}_{\text{FB}}$ is a centro-Hermitian matrix. In fact, it has been shown that $\widehat{\mathbf{R}}_{\text{FB}}$ is centro-Hermitian with an arbitrary source covariance matrix $\mathbb{S}$, and the $\widehat{\mathbf{R}}_{\text{FB}}$ has been used in various DOA estimation algorithms [36–38]. Using (44), it can be easily verified that

$$\begin{cases}\text{Re}^T\left(\widehat{\mathbf{R}}_{\text{FB}}\right)=\text{Re}\left(\widehat{\mathbf{R}}_{\text{FB}}\right) & \text{(a)}\\ \mathbb{J}\text{Re}\left(\widehat{\mathbf{R}}_{\text{FB}}\right)\mathbb{J}=\text{Re}\left(\widehat{\mathbf{R}}_{\text{FB}}\right), & \text{(b)}\end{cases} \tag{45}$$

which suggests that $\text{Re}\left(\widehat{\mathbf{R}}_{\text{FB}}\right)$ is a bisymmetric matrix. Therefore, we can use $\text{Re}\left(\widehat{\mathbf{R}}_{\text{FB}}\right)$ instead of the $\widehat{\mathbb{R}}_{\text{re}}$ to construct the proposed R-Capon cost function and to compute $\text{Re}^{-1}\left(\widehat{\mathbf{R}}_{\text{FB}}\right)$ by using the above two theorems in practice. □

Based on the above analysis, we compare the computational complexities between the conventional Capon and the proposed R-Capon in Table 1, in which J stands for the number of spectral sample points over the total angular field-of-view $[-\pi/2,\pi/2]$. Note that the complexities are given in terms of real-valued flops. Also note that only the two complexity-dominated steps (i.e., matrix inverse computation and spectral search) are considered for both the two algorithms.

For the matrix inverse computation step, as $\widehat{\mathbf{R}}$ is complex, the conventional Capon requires $4\times\mathcal{O}(M^3)$ flops to commutate $\widehat{\mathbf{R}}^{-1}$ [33]. However, R-Capon only need to compute the inverses of $\text{Re}\left(\widehat{\mathbf{R}}_{\text{FB}}\right)$. According to Theorem 1, Theorem 2 and Remark 5, $\text{Re}^{-1}\left(\widehat{\mathbf{R}}_{\text{FB}}\right)$ can be equivalently jointed by two sub-matrices $\widehat{\mathbb{H}}_1^{-1}$ and $\widehat{\mathbb{H}}_2^{-1}$ with $M=2k$ or by $\widehat{\mathbb{H}}_1^{-1}$ and $\widehat{\mathbb{H}}_3^{-1}$ with $M=2k+1$. Since the sub-matrices are of about half sizes $M/2\times M/2$, this term is significantly reduced to $2\times\mathcal{O}\left[(M/2)^3\right]=1/4\times\mathcal{O}(M^3)$ flops. It is worth noting that the FB averaging in (43) and the matrix jointing in (34) and (37) require no additional flops since they involve only element exchange and addition operations.

For the spectral search step, because $\widehat{\mathbf{R}}$ is complex and the conventional capon needs to search over $[-\pi/2,\pi/2]$ to find the spectral peaks, this term is given by $4J\times\mathcal{O}(M^2+M)$ [13]. As the spectral search involved in the proposed method is compressed into a half range $[-\pi/2,0]$ (or $[0,\pi/2]$), R-Capon need to compute only $J/2$ spectral points. Also note that $\text{Re}^{-1}\left(\widehat{\mathbf{R}}_{\text{FB}}\right)$ is real, the proposed method costs only $J/2\times\mathcal{O}(M^2+M)$ flops in the spectral search step.

Considering the slight flops required by the new method for solving the ambiguity problem can be omitted, we see from Table 1 that R-Capon has an obviously reduced complexity as compared to the conventional Capon.

Table 2
The proposed R-Capon algorithm.

- **Step 1**: Estimate $\widehat{\mathbf{R}}$ by (6), obtain $\widehat{\mathbf{R}}_{\text{FB}}$ by (43), and update $\widehat{\mathbb{R}}_{\text{re}}$ by $\widehat{\mathbb{R}}_{\text{re}}=\text{Re}\left(\widehat{\mathbf{R}}_{\text{FB}}\right)$.
- **Step 2**: If $M=2k$, compute $\widehat{\mathbb{H}}_1^{-1}$ and $\widehat{\mathbb{H}}_2^{-1}$ and get $\widehat{\mathbb{R}}_{\text{re}}^{-1}$ by (34); If $M=2k+1$, compute $\widehat{\mathbb{H}}_1^{-1}$ and $\widehat{\mathbb{H}}_3^{-1}$ and get $\widehat{\mathbb{R}}_{\text{re}}^{-1}$ by (37).
- **Step 3**: Search $f_{\text{R-Capon}}(\theta)$ over $[0,\pi/2]$ (or $[-\pi/2,0]$) to obtain the candidate angles $\widehat{\boldsymbol{\theta}}\triangleq\{\widehat{\theta}_1,\widehat{\theta}_2,\ldots,\widehat{\theta}_Q\}$, $Q\leq K$;
- **Step 4**: For each $\widehat{\theta}\in\widehat{\boldsymbol{\theta}}$, select the true DOA between $\widehat{\theta}$ and $-\widehat{\theta}$ by maximizing $\|\mathbf{a}^H(\theta)\widehat{\mathbf{R}}\mathbf{a}(\theta)\|^2$.

4.3. Summary of the proposed method

Detailed steps for implementing the proposed R-Capon algorithm fast DOA estimation with unknown number of signals are summarized in Table 2.

5. Simulation results

Numerical simulations with 500 independent Monte Carlo trials are conducted to assess the performance of the proposed R-Capon algorithm and compare it to the conventional Capon. For the root mean square error (RMSE) comparison, the Cramér-Rao Lower Bound (CRLB) given in [39] is applied as a common reference, and the RMSE is defined as

$$\text{RMSE}\triangleq\sqrt{\frac{1}{500}\sum_{i=1}^{500}\left(\widehat{\theta}_i-\theta\right)^2}, \tag{46}$$

where $\widehat{\theta}_i$ stands for the ith estimated value for θ. For K sources, the SNR is defined as

$$\text{SNR}\triangleq 10\log_{10}\left[\frac{P_{\text{avg}}}{\sigma_n^2}\right], \tag{47}$$

where $P_{\text{avg}}=\frac{1}{K}\sum_{l=1}^{K}P_k$ is the source average power and $P_k=E\left[\mathbf{s}_k^2(t)\right]$ is the power of the kth, $k\in[1,K]$ source. For a matrix $\mathbf{A}$, its condition number is given by [33]

$$\text{cond}(\mathbf{A})\triangleq\left|\frac{\lambda_{\max}(\mathbf{A})}{\lambda_{\min}(\mathbf{A})}\right|, \tag{48}$$

where $\lambda_{\max}(\mathbf{A})$ and $\lambda_{\min}(\mathbf{A})$ maximal and minimal eigenvalues of $\mathbf{A}$, respectively.

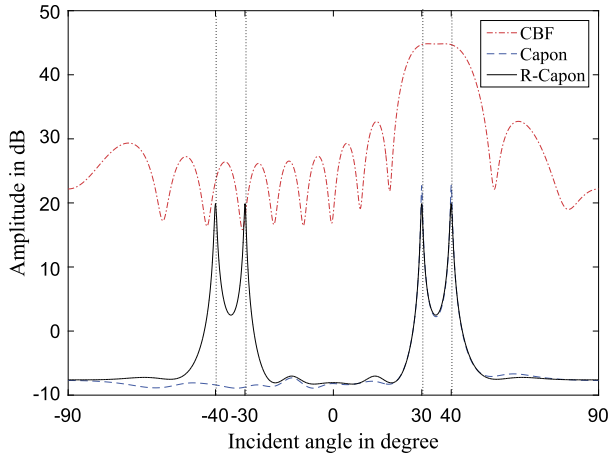

Fig. 1. Spectrums comparison, ULA, $M = 10$ sensors, SNR = 10 dB, $T = 100$ snapshots, $K = 2$ sources at $\theta_1 = 30°$ and $\theta_2 = 40°$.

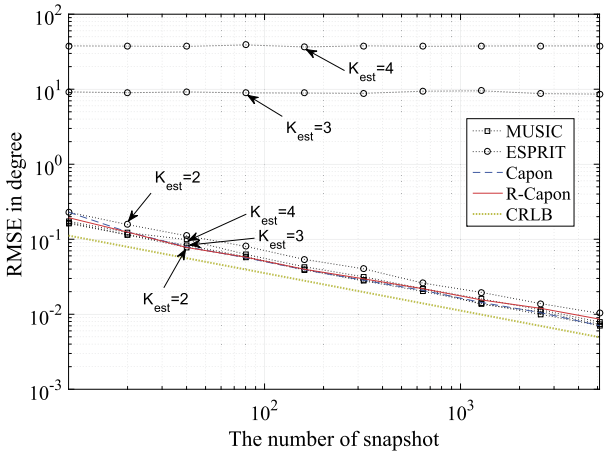

Fig. 3. RMSE against the number of snapshots respect to $\theta_2 = 30°$, ULA, $M = 12$ sensors, $K = 2$ signals at $\theta_1 = 20°$ and $\theta_2 = 30°$, SNR = 10 dB.

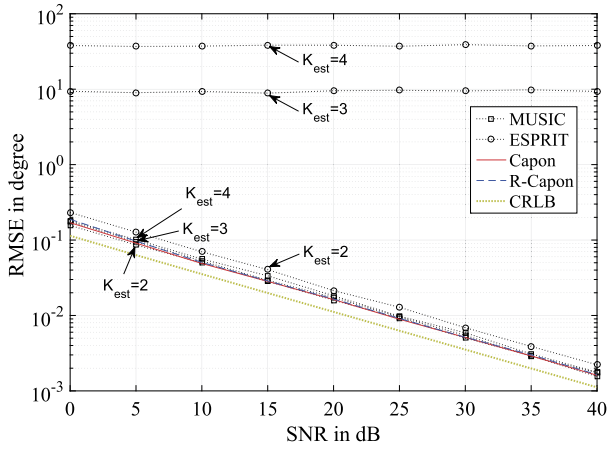

Fig. 2. RMSE against the SNR respect to $\theta_2 = 30°$, ULA, $M = 12$ sensors, $K = 2$ signals at $\theta_1 = 20°$ and $\theta_2 = 30°$, $T = 100$ snapshots.

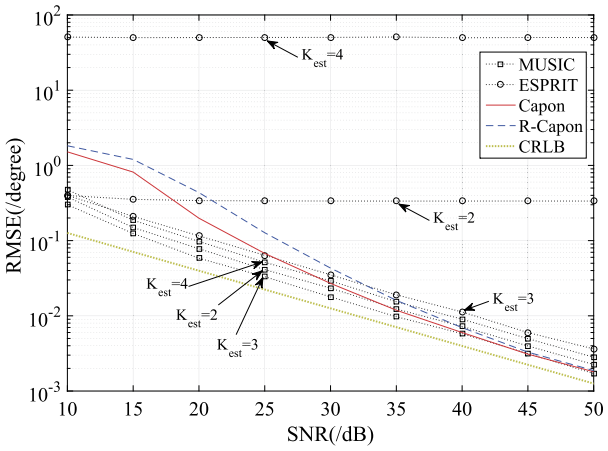

Fig. 4. RMSE against the SNR respect to $\theta_2 = 30°$, ULA, $M = 14$ sensors, $K = 3$ signals at $\theta_1 = 20°$, $\theta_2 = 30°$ and $\theta_3 = 33°$, $T = 100$ snapshots.

In the first simulation, we compare in Fig. 1 the spectrums of different algorithms including CBF [1], Capon [26] and the proposed R-Capon, where the simulation parameters are given in the figure caption. As was expected, it is seen from Fig. 1 that the proposed R-Capon show peaks at the true DOAs and their symmetrical mirrors simultaneously. This allows fast spectral search over half of the angular field-of-view. Since the CBF takes the maximums only at the directions of true DOAs, we can use the CBF to solve the ambiguity problem by using step 4) in Table 2.

In the second simulation, we compare the RMSE performances of diffident algorithms including the conventional Capon, the proposed R-Capon technique, MUSIC and ESPRIT, where $K = 2$ well-separated sources are considered. We use K_{est} to denote the estimated number of signal for MUSIC and ESPRIT, and set K_{est} with diffident values as control parameters for the two subspace-based methods. We first plot the RMSEs as functions of the SNR in Fig. 2, and next plot those as functions of the number of snapshots in Fig. 3. The simulation parameters are given in both captions of the two figures.

It is seen clearly from Fig. 2 that, with $T = 100$ over a wide range of SNR = 0 dB $\sim$ SNR = 40 dB, the proposed R-Capon provides a similar performance to the conventional Capon. With $K_{est} = K = 2$, meaning that MUSIC and ESPRIT works in idea scenario where the number of sources is correctly estimated, the proposed method shows close RMSEs to MUSIC, and it is much better ESPRIT. With $K_{est} \neq K$, meaning that MUSIC and ESPRIT works in worse scenario where the number of sources is incorrectly estimated, R-Capon outperforms both MUSIC and ESPRIT. This verifies the advantage of the proposed algorithm for DOA estimation with unknown number of signal over MUSIC and ESPRIT. On the other hand, with a moderate SNR = 10 dB, the similar superiority for R-Capon over MUSIC and ESPRIT can be observed again from Fig. 3, in which it is also seen that our method provides slightly better accuracy than the conventional with small T's within $T \leqslant 100$.

In the third simulation, we compare the RMSEs of Capon, R-Capon, MUSIC and ESPRIT, where $K = 3$ sources are considered and two of the three sources are assumed to be closely-spaced. We set K_{est} again with diffident values as control parameters for the two subspace-based methods, and plot RMSEs as functions of the SNR and as those of the number of snapshots in Fig. 4 and Fig. 5, respectively. The simulation parameters are given in both captions of the two figures.

It can seen clearly from Fig. 4 that the proposed method shows a similar performance to the standard Capon, but both Capon and R-Capon show worse accuracies than the MUSIC algorithm within SNR $<$ 35 dB, even the latter works with incorrectly estimated signal numbers $K_{est} = 2$ and $K_{est} = 4$. With sufficiently high SNRs such as SNR $\geqslant$ 35 dB, both Capon and R-Capon outperform MUSIC with $K_{est} = 2$ and $K_{est} = 4$. This is because only in high SNRs, the AOCM (and the R-AOCM) approximate to the noise subspace projection matrix [13] with no signal subspace leakage [40]. However, the proposed method shows much better performance than ESPRIT when the latter works with incorrectly estimated signal numbers $K_{est} = 2$ and $K_{est} = 4$. The above conclusions can be also observed

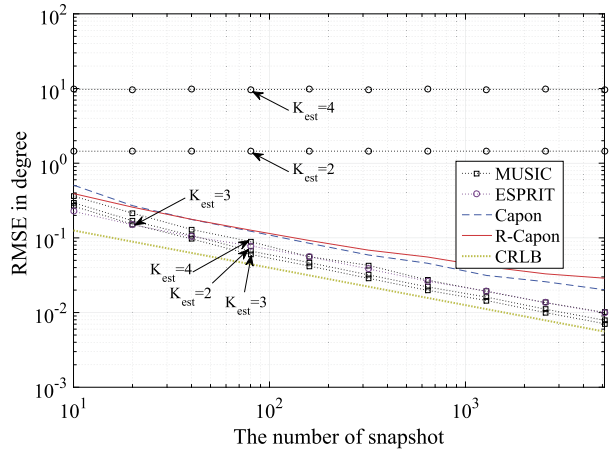

Fig. 5. RMSE against the number of snapshots respect to $\theta_2 = 30°$, ULA, $M = 14$ sensors, $K = 3$ signals at $\theta_1 = 20°$, $\theta_2 = 30°$ and $\theta_3 = 33°$, SNR = 20 dB.

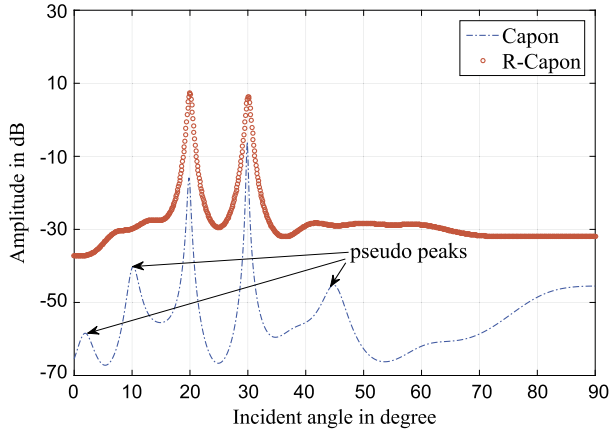

Fig. 6. Direction finding by Capon and the proposed R-Capon, ULA, $M = 14$ sensors, $K = 2$ signals at $\theta_1 = 20°$ and $\theta_2 = 30°$, $T = 20$ snapshots and SNR = 10 dB.

clearly from Fig. 5, in which it can be seen again that the proposed algorithm outperforms the conventional with small T's.

In the fourth simulation, we examine the performance of the new method with small T's. In Fig. 6, we compare the spectrums of the conventional Capon and the proposed R-Capon algorithms with a small number $T = 20$. It is observed from Fig. 6 that with only $T = 20$ snapshots, the conventional Capon shows pseudo peaks while R-Capon does not. Although Fig. 6 gives the result of only one trial, we find the pseudo peak is a recurrent phenomenon in the conventional Capon spectral.

To further confirm the results (with small T's) observed from Fig. 3, Fig. 5 and Fig. 6, we compare the condition number and rank of three matrix, $\widehat{\mathbf{R}}$, $\widehat{\mathbf{R}}_{\mathrm{FB}}$ and $\mathrm{Re}(\widehat{\mathbf{R}}_{\mathrm{FB}})$ in Fig. 7 and Fig. 8, respectively. The simulation parameters are given in both captions of the two figures. It is seen clearly from Fig. 7 and Fig. 8 that

$$\begin{cases} \mathrm{cond}(\widehat{\mathbf{R}}) > \mathrm{cond}(\widehat{\mathbf{R}}_{\mathrm{FB}}) > \mathrm{cond}[\mathrm{Re}(\widehat{\mathbf{R}}_{\mathrm{FB}})] & \text{(a)} \\ \mathrm{rank}(\widehat{\mathbf{R}}) \leqslant \mathrm{rank}(\widehat{\mathbf{R}}_{\mathrm{FB}}) \leqslant \mathrm{rank}[\mathrm{Re}(\widehat{\mathbf{R}}_{\mathrm{FB}})] & \text{(b)} \end{cases} \tag{49}$$

holds all along the varying range of number of snapshot. According to matrix theory, the condition number reflects how sensitive a function is to errors in the input, and big condition number generally means higher sensitivity [33]. For ideal $\mathbf{R}$ and $\mathrm{Re}(\mathbf{R}_{\mathrm{FB}})$, we have $\mathbf{a}^H(\theta)\mathbf{R}^{-1}\mathbf{a}(\theta) = 0$ and $\mathbf{a}^H(\theta)\mathrm{Re}^{-1}(\mathbf{R}_{\mathrm{FB}})\mathbf{a}(\theta) = 0$ at the look direction θ. With estimated errors in $\widehat{\mathbf{R}}$ and $\widehat{\mathbf{R}}_{\mathrm{FB}}$, both Capon and R-Capon show estimated errors accordingly, and therefore, (49a) is the underlying reasons that the proposed technique shows enhanced performance as compared to Capon with small T's. On the other hand, It is also seen from Fig. 8 that the condition for equality in (49b) is $T \geqslant 12$. This is because we in fact have $\mathrm{rank}(\widehat{\mathbf{R}}) = \mathrm{rank}(\widehat{\mathbf{X}}) = \min(M, T)$. Thus, the results in Fig. 7 and Fig. 8 confirms again the enhanced performances by the proposed method as compared to the standard Capon.

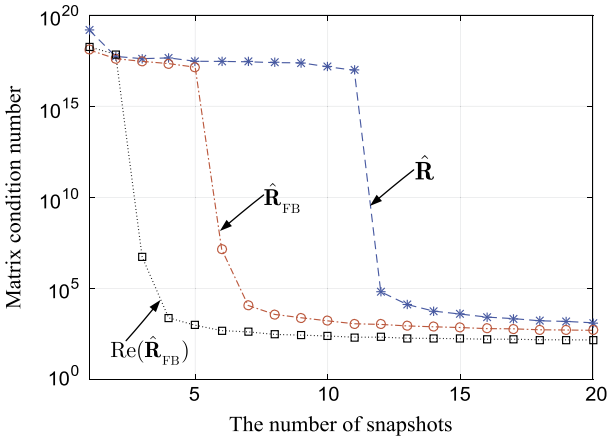

Fig. 7. Matrix condition number against the number of snapshot, ULA, $M = 12$ sensors, SNR = 10 dB, $K = 2$ sources at $\theta_1 = 30°$ and $\theta_2 = 40°$.

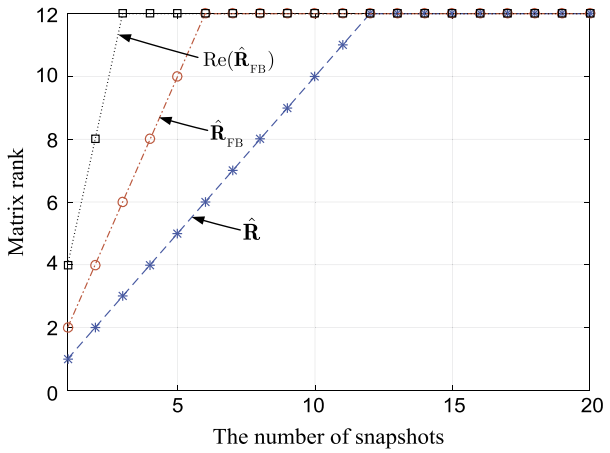

Fig. 8. Matrix rank against the number of snapshot, ULA, $M = 12$ sensors, SNR = 10 dB, $K = 2$ sources at $\theta_1 = 30°$ and $\theta_2 = 40°$.

Table 3
Comparison of CPU time in second.

Items	$M = 8$	$M = 12$	$M = 16$	$M = 20$	$M = 24$
MUSIC	1.3358	2.5361	2.6361	2.8725	3.0456
ESPRIT	0.0211	0.0212	0.0420	0.0571	0.0678
Capon	1.8017	3.1400	3.3097	3.2956	3.5283
R-Capon	0.2003	0.4121	0.5201	0.5510	0.5806

In the last simulation, we investigate the computational efficiency of R-Capon. In Table 3, we compare the CPU times of Capon, R-Capon, MUSIC and ESPRIT against the number of sensors using a ULA. The simulation parameters are set as SNR = 10 dB, $T = 100$, $K = 2$, $\theta_1 = 30°$ and $\theta_2 = 35°$. The CPU times are given by running the Matlab codes on a PC with the same configurations in the same environment. It can be seen from Table 3 that R-Capon costs much lower CPU times than both MUSIC and Capon, which are consistent with our expectations.

6. Conclusions

We have proposed a novel R-Capon algorithm for DOA estimation without detecting the number of sources. R-Capon exploits only the R-AOCM instead of the entire AOCM to reduce the complexity by real-valued computations. Further more, the inverse of the R-AOCM is proven to be equivalently jointed by two sub-matrices of about half sizes, which further reduces the complexity significantly. Theoretical analysis and simulations demonstrate that R-Capon also outperforms Capon with small numbers of snapshots as there is a rank enhancement by R-Capon as compared to the conventional Capon.

7. Acknowledgments

This work is supported by National Natural Science Foundation of China (61501142), Science and Technology Program of Wei-Hai, Project Supported by Discipline Construction Guiding Foundation in Harbin Institute of Technology (Weihai) (WH20160107) and the Fundamental Research Funds for the Central Universities (HIT.NSRIF.201725).

Appendix A. Proof of Theorem 1

Because $\mathbb{R}_{\rm re}$ is a $2k\times 2k$ matrix, we can divide $\mathbb{R}_{\rm re}$ into four $k\times k$ sub-matrices as

$$\mathbb{R}_{\rm re}=\begin{bmatrix}(\mathbb{R}_{\rm re})_{11} & (\mathbb{R}_{\rm re})_{12}\\ (\mathbb{R}_{\rm re})_{21} & (\mathbb{R}_{\rm re})_{22}\end{bmatrix}. \tag{A.1}$$

Since $\mathbb{R}_{\rm re}^T=\mathbb{R}_{\rm re}$, we have

$$(\mathbb{R}_{\rm re})_{12}=(\mathbb{R}_{\rm re})_{21}^T. \tag{A.2}$$

Inserting (A.1) into (32b) and using (A.2) leads to

$$\begin{aligned}\mathbb{J}\mathbb{R}_{\rm re}\mathbb{J}&=\begin{bmatrix}&\mathbb{J}\\ \mathbb{J}&\end{bmatrix}\begin{bmatrix}(\mathbb{R}_{\rm re})_{11} & (\mathbb{R}_{\rm re})_{21}^T\\ (\mathbb{R}_{\rm re})_{21} & (\mathbb{R}_{\rm re})_{22}\end{bmatrix}\begin{bmatrix}&\mathbb{J}\\ \mathbb{J}&\end{bmatrix}\\ &=\begin{bmatrix}\mathbb{J}(\mathbb{R}_{\rm re})_{22}\mathbb{J} & \mathbb{J}(\mathbb{R}_{\rm re})_{21}\mathbb{J}\\ \mathbb{J}(\mathbb{R}_{\rm re})_{21}^T\mathbb{J} & \mathbb{J}(\mathbb{R}_{\rm re})_{11}\mathbb{J}\end{bmatrix}\\ &=\begin{bmatrix}(\mathbb{R}_{\rm re})_{11} & (\mathbb{R}_{\rm re})_{21}^T\\ (\mathbb{R}_{\rm re})_{21} & (\mathbb{R}_{\rm re})_{22}\end{bmatrix}=\mathbb{R}_{\rm re}.\end{aligned} \tag{A.3}$$

Notice that $\mathbb{J}^2=\mathbb{I}$, it follows from (A.3) that

$$\begin{cases}(\mathbb{R}_{\rm re})_{22}=\mathbb{J}(\mathbb{R}_{\rm re})_{11}\mathbb{J} & \text{(a)}\\ \mathbb{J}(\mathbb{R}_{\rm re})_{21}=(\mathbb{R}_{\rm re})_{21}^T\mathbb{J}. & \text{(b)}\end{cases} \tag{A.4}$$

It can seen clearly from (A.2) and (A.4) that the two dependent sub-matrices $(\mathbb{R}_{\rm re})_{12}$ and $(\mathbb{R}_{\rm re})_{22}$ in (A.1) can be removed without the division, and hence we obtain (33).

To prove (34), let us introduce the following $2k\times 2k$ matrix

$$\mathbb{P}\triangleq\frac{1}{\sqrt{2}}\begin{bmatrix}\mathbb{I} & \mathbb{I}\\ -\mathbb{J} & \mathbb{J}\end{bmatrix}. \tag{A.5}$$

Using (A.4b) and (33), it can easily shown that

$$\begin{aligned}\mathbb{P}^T\mathbb{R}_{\rm re}\mathbb{P}&=\frac{1}{2}\begin{bmatrix}\mathbb{I} & -\mathbb{J}\\ \mathbb{I} & \mathbb{J}\end{bmatrix}\begin{bmatrix}(\mathbb{R}_{\rm re})_{11} & (\mathbb{R}_{\rm re})_{21}^T\\ (\mathbb{R}_{\rm re})_{21} & \mathbb{J}(\mathbb{R}_{\rm re})_{11}\mathbb{J}\end{bmatrix}\begin{bmatrix}\mathbb{I} & \mathbb{I}\\ -\mathbb{J} & \mathbb{J}\end{bmatrix}\\ &=\begin{bmatrix}(\mathbb{R}_{\rm re})_{11}-\mathbb{J}(\mathbb{R}_{\rm re})_{12} & \mathbf{0}\\ \mathbf{0} & (\mathbb{R}_{\rm re})_{11}+\mathbb{J}(\mathbb{R}_{\rm re})_{12}\end{bmatrix}\\ &=\begin{bmatrix}\mathbb{H}_1 & \mathbf{0}\\ \mathbf{0} & \mathbb{H}_2\end{bmatrix}.\end{aligned} \tag{A.6}$$

Notice that $\mathbb{P}^{-1}=\mathbb{P}^T$, we obtain from (A.6) that

$$\begin{aligned}\mathbb{R}_{\rm re}^{-1}&=\mathbb{P}\begin{bmatrix}\mathbb{H}_1^{-1} & \mathbf{0}\\ \mathbf{0} & \mathbb{H}_2^{-1}\end{bmatrix}\mathbb{P}^T\\ &=\frac{1}{2}\begin{bmatrix}\mathbb{I} & \mathbb{I}\\ -\mathbb{J} & \mathbb{J}\end{bmatrix}\begin{bmatrix}\mathbb{H}_1^{-1} & \mathbf{0}\\ \mathbf{0} & \mathbb{H}_2^{-1}\end{bmatrix}\begin{bmatrix}\mathbb{I} & -\mathbb{J}\\ \mathbb{I} & \mathbb{J}\end{bmatrix}\\ &=\frac{1}{2}\begin{bmatrix}\mathbb{H}_1^{-1}+\mathbb{H}_2^{-1} & \left(\mathbb{H}_2^{-1}-\mathbb{H}_1^{-1}\right)\mathbb{J}\\ \mathbb{J}\left(\mathbb{H}_2^{-1}-\mathbb{H}_1^{-1}\right) & \mathbb{J}\left(\mathbb{H}_1^{-1}+\mathbb{H}_2^{-1}\right)\mathbb{J}\end{bmatrix},\end{aligned} \tag{A.7}$$

which completes the proof.

Appendix B. Proof of Theorem 2

Because $\mathbb{R}_{\rm re}$ is of dimensions $(2k+1)\times(2k+1)$ and notice that $\mathbb{R}_{\rm re}^T=\mathbb{R}_{\rm re}$, we can divide $\mathbb{R}_{\rm re}$ as

$$\mathbb{R}_{\rm re}=\begin{bmatrix}(\mathbb{R}_{\rm re})_{11} & \mathbb{b} & (\mathbb{R}_{\rm re})_{21}^T\\ \mathbb{b}^T & a & \mathbb{c}^T\\ (\mathbb{R}_{\rm re})_{21} & \mathbb{c} & (\mathbb{R}_{\rm re})_{22}\end{bmatrix}, \tag{B.1}$$

where a is a scalar, $\mathbb{b}$ and $\mathbb{c}$ are two $k\times 1$ vector, $(\mathbb{R}_{\rm re})_{11}$, $(\mathbb{R}_{\rm re})_{21}$ and $(\mathbb{R}_{\rm re})_{22}$ are three $k\times k$ sub-matrices. Inserting (B.1) into (32b), we obtain

$$\begin{aligned}\mathbb{J}\mathbb{R}_{\rm re}\mathbb{J}&=\begin{bmatrix}&&\mathbb{J}\\ &1&\\ \mathbb{J}&&\end{bmatrix}\begin{bmatrix}(\mathbb{R}_{\rm re})_{11} & \mathbb{b} & (\mathbb{R}_{\rm re})_{21}^T\\ \mathbb{b}^T & a & \mathbb{c}^T\\ (\mathbb{R}_{\rm re})_{21} & \mathbb{c} & (\mathbb{R}_{\rm re})_{22}\end{bmatrix}\\ &\quad\times\begin{bmatrix}&&\mathbb{J}\\ &1&\\ \mathbb{J}&&\end{bmatrix}\\ &=\begin{bmatrix}\mathbb{J}(\mathbb{R}_{\rm re})_{22}\mathbb{J} & \mathbb{J}\mathbb{c} & \mathbb{J}(\mathbb{R}_{\rm re})_{21}\mathbb{J}\\ \mathbb{c}^T\mathbb{J} & a & \mathbb{b}^T\mathbb{J}\\ \mathbb{J}(\mathbb{R}_{\rm re})_{21}^T\mathbb{J} & \mathbb{J}\mathbb{b} & \mathbb{J}(\mathbb{R}_{\rm re})_{11}\mathbb{J}\end{bmatrix}\\ &=\begin{bmatrix}(\mathbb{R}_{\rm re})_{11} & \mathbb{b} & (\mathbb{R}_{\rm re})_{21}^T\\ \mathbb{b}^T & a & \mathbb{c}^T\\ (\mathbb{R}_{\rm re})_{21} & \mathbb{c} & (\mathbb{R}_{\rm re})_{22}\end{bmatrix}=\mathbb{R}_{\rm re},\end{aligned} \tag{B.2}$$

which gives

$$\begin{cases}(\mathbb{R}_{\rm re})_{22}=\mathbb{J}(\mathbb{R}_{\rm re})_{11}\mathbb{J} & \text{(a)}\\ \mathbb{J}(\mathbb{R}_{\rm re})_{21}=(\mathbb{R}_{\rm re})_{21}^T\mathbb{J} & \text{(b)}\\ \mathbb{c}=\mathbb{J}\mathbb{b}. & \text{(c)}\end{cases} \tag{B.3}$$

Using (B.3), the two dependent elements $(\mathbb{R}_{\rm re})_{22}$ and $\mathbb{c}$ can be removed, and we obtain (36) immediately.

Introduce the following $(2k+1)\times(2k+1)$ matrix

$$\mathbb{Q}\triangleq\frac{1}{\sqrt{2}}\begin{bmatrix}\mathbb{I} & \mathbf{0} & \mathbb{I}\\ \mathbf{0} & \sqrt{2} & \mathbf{0}\\ -\mathbb{J} & \mathbf{0} & \mathbb{J}\end{bmatrix}, \tag{B.4}$$

with its inverse given by $\mathbb{Q}^{-1}=\mathbb{Q}^T$. Using $\mathbb{J}^2=\mathbb{I}$, (36) and (B.3), it is straightforward to shown that

$$\mathbb{Q}^T\mathbb{R}_{\rm re}\mathbb{Q}=\begin{bmatrix}\mathbb{H}_1 & \mathbf{0} & \mathbf{0}\\ \mathbf{0} & a & \sqrt{2}\mathbb{b}^T\\ \mathbf{0} & \sqrt{2}\mathbb{b} & \mathbb{H}_2\end{bmatrix}=\begin{bmatrix}\mathbb{H}_1 & \mathbf{0}\\ \mathbf{0} & \mathbb{H}_3\end{bmatrix}, \tag{B.5}$$

where $\mathbb{H}_2$ is a $k\times K$ sub-matrix defined in (35-2). Notice that $\mathbb{Q}$ can be divided as

$$\mathbb{Q} = \frac{1}{\sqrt{2}} \begin{bmatrix} \mathbb{I} & \mathbb{K}_1 \\ \mathbb{K}_2 & \mathbb{L} \end{bmatrix}, \tag{B.6}$$

we obtain from (B.5) that

$$\begin{aligned} \mathbb{R}_{re}^{-1} &= \mathbb{Q} \begin{bmatrix} \mathbb{H}_1^{-1} & \mathbf{0} \\ \mathbf{0} & \mathbb{H}_3^{-1} \end{bmatrix} \mathbb{Q}^T \\ &= \frac{1}{2} \begin{bmatrix} \mathbb{I} & \mathbb{K}_1 \\ \mathbb{K}_2 & \mathbb{L} \end{bmatrix} \begin{bmatrix} \mathbb{H}_1^{-1} & \mathbf{0} \\ \mathbf{0} & \mathbb{H}_3^{-1} \end{bmatrix} \begin{bmatrix} \mathbb{I} & \mathbb{K}_2^T \\ \mathbb{K}_1^T & \mathbb{L} \end{bmatrix} \\ &= \frac{1}{2} \begin{bmatrix} \mathbb{H}_1^{-1} + \mathbb{K}_1 \mathbb{H}_3^{-1} \mathbb{K}_1^T & \mathbb{H}_1^{-1} \mathbb{K}_2^T + \mathbb{K}_1 \mathbb{H}_3^{-1} \mathbb{L} \\ \mathbb{K}_2 \mathbb{H}_1^{-1} + \mathbb{L} \mathbb{H}_3^{-1} \mathbb{K}_1^T & \mathbb{K}_2 \mathbb{H}_1^{-1} \mathbb{K}_2^T + \mathbb{L} \mathbb{H}_3^{-1} \mathbb{L}^T \end{bmatrix}, \end{aligned} \tag{B.7}$$

and the proof is completed.

References

[1] J. Krim, M. Viberg, Two decades of array signal processing research: the parametric approach, IEEE Signal Process. Mag. 13 (3) (Jul. 1996) 67–94.
[2] J.C. Chen, K. Yao, R.E. Hudson, Source localization and beamforming, IEEE Signal Process. Mag. 19 (2) (Mar. 2002) 30–39.
[3] R.O. Schmidt, Multiple emitter location and signal parameter estimation, IEEE Trans. Antennas Propag. 34 (3) (Mar. 1986) 276–280.
[4] R. Roy, T. Kailath, ESPRIT-estimation of signal parameters via rotational invariance techniques, IEEE Trans. Signal Process. 37 (7) (Jul. 1989) 984–995.
[5] F.G. Yan, M. Jin, X.L. Qiao, Low-complexity DOA estimation based on compressed MUSIC and its performance analysis, IEEE Trans. Signal Process. 61 (8) (April 2013) 1915–1930.
[6] F.G. Yan, Y. Shen, M. Jin, Fast DOA estimation based on a split subspace decomposition on the array covariance matrix, Signal Process. 115 (Oct. 2015) 1–8.
[7] K.C. Huarng, C.C. Yeh, A unitary transformation method for angle-of-arrival estimation, IEEE Trans. Signal Process. 39 (April 1991) 975–977.
[8] F.G. Yan, M. Jin, X.L. Qiao, Source localization based on symmetrical MUSIC and its statistical performance analysis, Sci. China Inf. Sci. 56 (2013) 062307, https://doi.org/10.1007/s11432-013-4841-6.
[9] F.G. Yan, M. Jin, S. Liu, X.L. Qiao, Real-valued MUSIC for efficient direction estimation with arbitrary array geometries, IEEE Trans. Signal Process. 62 (6) (Mar. 2014) 1548–1560.
[10] F.G. Yan, Y. Shen, M. Jin, X.L. Qiao, Computationally efficient direction finding using polynomial rooting with reduced-order and real-valued computations, J. Syst. Eng. Electron. 27 (4) (Aug. 2016) 739–745.
[11] S. Kung, K.S. Arun, D.V.B. Rao, Statespace and singularvalue decomposition-based approximation methods for the harmonic retrieval problem, J. Opt. Soc. Am. 73 (Dec. 1983) 1799–1811.
[12] F.G. Yan, T. Jin, M. Jin, Y. Shen, Subspace-based direction-of-arrival estimation using centro-symmetrical arrays, Electron. Lett. 27 (11) (Oct. 2016) 1895–1896.
[13] Ying Zhang, Boon Poh Ng, MUSIC-like DOA estimation without estimating the number of sources, IEEE Trans. Signal Process. 58 (3) (March 2010) 1668–1676.
[14] V.V. Reddy, B.P. Ng, A.W.H. Khong, Insights into MUSIC-like algorithm, IEEE Trans. Signal Process. 61 (10) (May 15, 2013) 2551–2556.
[15] V.V. Reddy, M. Mubeen, B.P. Ng, Reduced-complexity super-resolution DOA estimation with unknown number of sources, IEEE Signal Process. Lett. 22 (6) (June 2015) 772–776.
[16] W. Xie, F. Wen, J. Liu, Q. Wan, Source association, DOA, and fading coefficients estimation for multipath signals, IEEE Trans. Signal Process. 65 (11) (June 1, 2017) 2773–2786.
[17] B. Picinbono, On circularity, IEEE Trans. Signal Process. 42 (12) (Dec. 1994) 3473–3482.
[18] P. Chargé, Y. Wang, J. Saillard, A non-circular sources direction finding method using polynomial rooting, Signal Process. 81 (8) (2001) 1765–1770.
[19] H. Abeida, J.P. Delmas, MUSIC-like estimation of direction of arrival for noncircular sources, IEEE Trans. Signal Process. 54 (7) (July 2006) 2678–2690.
[20] M. Wax, T. Kailath, Detection of signals by information theoretic criteria, IEEE Trans. Acoust. Speech Signal Process. 33 (3) (Apr. 1985) 387–392.
[21] W.-J. Zeng, X.-L. Li, X.-D. Zhang, Direction-of-arrival estimation based on the joint diagonalization structure of multiple fourthorder cumulant matrices, IEEE Signal Process. Lett. 16 (3) (Mar. 2009) 164–167.
[22] C.Y. Qi, Y.S. Zhang, Y. Han, X.H. Chen, An algorithm on high resolution DOA estimation with unknown number of signal sources, in: Proc. 4th Int. Conf. Microw. Millimeter Wave Technol., ICMMT, Aug. 18–21, 2004, pp. 227–230.
[23] M.N. Jin, Y.J. Zhao, D.H. Li, Joint source number detection and DOA estimation via reversible jump MCMC, in: Proc. Microw. MillimeterWave Technol. Pacific-AsiaWorkshop Computational Intell. Ind. Appl., PACIIA, 1 Dec. 19–20, 2008, pp. 859–863.
[24] J.C. Chen, K. Yao, R.E. Hudson, Source localization and beamforming, IEEE Signal Process. Mag. 19 (2) (Mar. 2002) 30–39.
[25] N. Zou, A. Nehorai, Circular acoustic vector-sensor array for mode beamforming, IEEE Trans. Signal Process. 57 (8) (Aug. 2009) 3041–3052.
[26] J. Capon, High resolution frequency-wavenumber spectrum analysis, Proc. IEEE 57 (8) (Aug. 1969) 1408–1418.
[27] J.X. Wu, T. Wang, Z.Y. Suo, Z. Bao, DOA estimation for ULA by spectral Capon rooting method, Electron. Lett. 45 (1) (January 1 2009) 84–85.
[28] X. Zhang, D. Xu, Angle estimation in bistatic MIMO radar using improved reduced dimension Capon algorithm, J. Syst. Eng. Electron. 24 (1) (Feb. 2013) 84–89.
[29] W.J. Zeng, X.L. Li, High-resolution multiple wideband and nonstationary source localization with unknown number of sources, IEEE Trans. Signal Process. 58 (6) (June 2010) 3125–3136.
[30] G.T. Pham, P. Loubaton, P. Vallet, Performance analysis of spatial smoothing schemes in the context of large arrays, IEEE Trans. Signal Process. 64 (1) (Jan. 1 2016) 160–172.
[31] L.C. Godara, Application of antenna arrays to mobile communications. II. Beamforming and direction-of-arrival considerations, Proc. IEEE 85 (8) (Aug. 1997) 1195–1245.
[32] J.W. Shin, Y.J. Lee, H.N. Kim, Reduced-complexity maximum likelihood direction-of-arrival estimation based on spatial aliasing, IEEE Trans. Signal Process. 62 (24) (Dec. 2014) 6568–6581.
[33] G.H. Golub, C.H. Van Loan, Matrix Computations, The Johns Hopkins University Press, Baltimore, MD, 1996.
[34] D.A. Linebarger, R.D. DeGroat, E.M. Dowling, Efficient direction-finding methods employing forward–backward averaging, IEEE Trans. Signal Process. 42 (8) (Aug. 1994) 2136–2145.
[35] P. Stoica, M. Jansson, On forward–backward MODE for array signal processing, Digit. Signal Process. 7 (4) (Oct. 1997) 239–252.
[36] M. Pesavento, A.B. Gershman, M. Haardt, Unitary root-MUSIC with a real-valued eigendecomposition: a theoretical and experimental performance study, IEEE Trans. Signal Process. 48 (5) (May 2000) 1306–1314.
[37] M. Pesavento, A.B. Gershman, M. Haardt, Unitary root-MUSIC with a real-valued eigendecomposition: a theoretical and experimental performance study, IEEE Trans. Signal Process. 48 (5) (May 2000) 1306–1314.
[38] N. Yilmazer, J. Koh, T.K. Sarkar, Utilization of a unitary transform for efficient computation in the matrix pencil method to find the direction of arrival, IEEE Trans. Signal Process. 54 (Jan. 2006) 175–181.
[39] P. Stoica, A. Nehorai, Performance study of conditional and unconditional direction-of-arrival estimation, IEEE Trans. Acoust. Speech Signal Process. 38 (Oct. 1990) 1783–1795.
[40] M. Shaghaghi, S.A. Vorobyov, Subspace leakage analysis and improved DOA estimation with small sample size, IEEE Trans. Signal Process. 63 (12) (June 15, 2015) 3251–3265.

Feng-Gang Yan received the Ph. D. degrees in information and communication engineering from Harbin Institute of Technology, Harbin, China, in 2014. From July 2008 to March 2011, he was a research associate of the Fifth Research Institute of China Aerospace Science and Technology Corporation (CASC), where his researches were mainly focused on the processing of remote sensing images. Since October 2015, Dr. Yan became an Associate Professor of the Department of Electronics information Engineering, Harbin Institute of Technology at Weihai, China. His current research interests include array signal processing and statistical performance analysis.

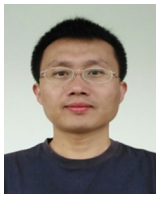

Jun Wang was born in China in 1976. He received the Ph.D. degrees in information and communication engineering from Harbin Institute of Technology, Harbin, China, in 2014. Since 2015, he has been an Associate Professor of the Department of Electronics information Engineering, Harbin Institute of Technology at Weihai, Weihai, China. His current research interests mainly focus on radar signal processing.

Shuai Liu was born in Heilongjiang Province, China, in 1980. He received the B.E. and M.S. degrees from Northwestern Polytechnical University China, in 2002 and 2005, respectively, and received the Ph.D degree in information and communication engineering from Harbin Institute of Technology (HIT), China, in 2013. Since 2013, he has been an Associate Professor of The School of Information and Electricity Engineering, HIT, Weihai, China. His current interests are in the area of conformal array and polarization sensitive array signal processing.

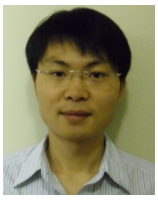

Bin Cao received his PhD (2013), master (2009), and bachelor (2007) degrees from Harbin Institute of Technology (HIT), China, all in Information and Communication Engineering. He has been a visiting student of University of Waterloo from 2010 to 2012, Canada. From 2014–2016, he worked as a postdoctoral fellow at HIT Shenzhen. From 2016, he has been an associate professor at HIT Shenzhen. His research interests include signal processing for wireless communications, cognitive radio networking, and resource allocation for wireless networks.

Ming Jin was born in Liaoning Province, China, in 1968. He received the B.E., M.S., and ph.D degree in information and communication engineering from Harbin Institute of Technology, China, in 1990, 1998 and 2004, respectively. From 1998 to 2004, He was with the Department of Electronics information Engineering, Harbin Institute of Technology. Since 2006, he became a Professor of The School of Information and Electricity Engineering, Harbin Institute of Technology at Weihai. His current interests include array signal processing and radar polarimetry.